J. Chem. Sci. (2026) 138:15
https://doi.org/10.1007/s12039-026-02477-z

REGULAR ARTICLE

Two-step seed-mediated growth for the reproducible synthesis of high quality gold nanorods

KUN-PENG WANG, JIE LIU*, XI CHEN, GUI-LIN WU, ER-JI ZHANG and TIAN-SONG DENG*

School of Electronics and Information Engineering, Hangzhou Dianzi University, Hangzhou 310018, People's Republic of China
*Corresponding authors. JIE LIU: liujie4209@hdu.edu.cn, TIAN-SONG DENG: dengts@pku.edu.cn

MS received 13 March 2025; revised 31 July 2025; accepted 14 August 2025

Abstract. Gold nanorods, as a type of anisotropic nanoparticles, require uniformity for their properties and applications. Here, we demonstrate the successful preparation of well-dispersed and uniformly shaped GNRs through a two-step seed-mediated growth method by separating the symmetry breaking of seeds from subsequent growth. We determined that adding the first growth solution (Solution A) into the second growth solution (Solution B) after 30 min was optimal, and monitored the growth progress by recording the growth status every 30 min, observing that the growth of Solution A (150 min) and Solution B (210 min) essentially ceased. Furthermore, by adjusting the seed quantity, silver ion content, and pH value of the growth solution in each step, we could tune the wavelength of the localized surface plasmon resonance (LSPR) peak within the range of 668 to 1020 nm. Additionally, the trend of overall electric field intensity variations were determined through finite difference time domain (FDTD) simulations. We believe that this approach will further facilitate practical applications of GNRs research, as these applications rely on the high uniformity of GNRs.

Keywords. Gold nanorods; two-step; seed-mediated; localized surface plasmon resonance.

1. Introduction

Gold nanorods (GNRs) have garnered significant attention due to their unique optical absorption spectrum characteristics and their enormous potential in fields such as biomedical applications,[1–3] photothermal conversion,[4–6] photonics,[7–9] and optoelectronic devices.[10–12] Control of GNRs' shape and size directly influences their optical,[13–15] electrical,[16–18] and magnetic properties,[15,19,20] thereby determining their potential applications in optical imaging,[21–23] sensors,[24–26] drug delivery[27–29] and other fields. However, the synthesis of GNRs faces challenges such as uniformity in shape, consistency in size, and controllability of optical properties.[30–33] Particularly in GNR synthesis, achieving the desired absorption spectrum range often requires controlling their aspect ratio (AR), which poses challenges in obtaining highly uniform GNRs.[34] Moreover, the size distribution of GNRs profoundly affects their properties and applications.[35] Therefore, developing an effective method to prepare highly uniform GNRs while achieving precise control over their shape and size is of significant scientific and practical importance.

The uniformity of GNRs primarily encompasses three aspects: shape, optical properties and size. In the context of GNR synthesis, shape uniformity refers to the proportion of nanoscale particles with rod-like shapes in the final product.[36] The higher the proportion of rod-like particles in the product, the better the shape uniformity. The second aspect is optical uniformity, which requires the longitudinal localized surface plasmon resonance (LSPR) absorption peak of GNRs to be as narrow as possible, quantified by the full width at half maximum (FWHM).[37] The efficiency of GNR samples in absorbing monochromatic light is related to the width of their longitudinal LSPR absorption peak, which is crucial for optical applications such as photothermal conversion and

Supplementary Information: The online version contains supplementary material at https://doi.org/10.1007/s12039-026-02477-z and https://www.ias.ac.in/chemsci.

Published online: 23 February 2026

therapy. The FWHM of the longitudinal LSPR absorption peak mainly depends on the distribution of the aspect ratio of GNRs rather than their absolute size. In other words, GNR samples with narrow LSPR peaks do not necessarily need to be monodisperse in size. The third aspect is size uniformity, requiring the synthesized GNRs to have identical dimensions for consistency. High size uniformity is a prerequisite for precisely controlling the shape and optical properties of GNRs.[38] Size uniformity is often accompanied by good optical uniformity, and as size uniformity increases, the distribution of aspect ratios of GNRs becomes narrower. In some applications, strict requirements are placed on size uniformity, such as self-assembling GNRs into large-scale two-dimensional arrays as highly reproducible surface-enhanced Raman scattering (SERS) substrates.[7,39] Many studies are dedicated to finding a synthesis method capable of mass-producing GNRs while meeting the requirements for shape, optical properties, and size uniformity. However, in the existing methods, achieving precise control over the shape and size of GNRs remains a challenging issue.

The two-step growth method is a primary approach for synthesizing elongated GNRs or gold nanowires.[40–42] For instance, Liz-Marzán and group separated the symmetry-breaking process from the seeded growth process: first, they prepared small-sized AuNRs with high yield in the presence of the surfactant hexadecyltrimethylammonium bromide and n-decanol (as a co-surfactant); then, these small-sized AuNRs were used as seeds to grow high-quality AuNR colloids. This approach resulted in uniform AuNR colloids with narrow plasmonic absorption bands ranging from 600 to 1270 nm.[30] Wang *et al.*[43] synthesized nanorods and nanowires ranging in length from 700 nm to 4.5 μm, with the longest nanowires reaching up to 6 μm. These nanowires maintained relatively thin average diameters of 33–53 nm. Recent studies have shown that this method can also be utilized for synthesizing nanoparticles with improved uniformity. For example, through two-step growth, uniform magnetic nanoparticles (Fe_3O_4) and uniform gold nanospheres with sizes ranging from 10 to 200 nm and a standard deviation below 10% have been successfully synthesized.[44] Murphy's team has developed a multi-step growth method for synthesizing pentatwinned GNRs with high aspect ratios (> 10).[45] However, due to the lower seed uniformity, the purity of the synthesized GNRs is also relatively low, resulting in poorer uniformity. Inspired by these achievements, we hypothesized that the two-step growth method could also effectively enhance the size uniformity of single-crystal GNRs.

Based on this concept, we propose a method for synthesizing GNRs with improved uniformity using a two-step seed-mediated growth approach. Building on the one-step growth method, we separate the symmetry-breaking of seeds from the subsequent non-uniform growth process, thereby conducting the growth in two steps. By monitoring the growth time, we determined the optimal growth time for adding the solution from the first step (bottle A) into the solution from the second step (bottle B), as well as the final completion time for both steps. In each step, we investigated the effects of varying seed volume, pH value, and silver ion content on the tunability and uniformity of the products. The optical properties and size uniformity of the products after each growth step were evaluated using UV-visible spectroscopy and transmission electron microscopy (TEM). Experimental results demonstrate a significant improvement in the uniformity of the final products through the two-step growth method. Additionally, by adjusting the tested experimental parameters, the size and LSPR absorption of the GNRs can be tuned across a wide range.

2. Experimental

2.1 *Materials*

All chemicals were obtained from commercial suppliers and used without further purification. Hexadecyltrimethylammonium bromide (CTAB, > 99.0%) was purchased from TCI America. Chloroauric acid ($HAuCl_4$), L-ascorbic acid (AA, > 99.99%) and hydrochloric acid (HCl, 37 wt.% in water) were purchased from Shanghai Macklin Biochemical Technology Co., Ltd. Silver nitrate ($AgNO_3$, > 99.8%), sodium oleate (NaOL, > 99.88%) and sodium borohydride ($NaBH_4$, > 98%) were purchased from Shanghai Aladdin Biochemical Technology Co., Ltd. Ultrapure water (> 18.2 MΩ) obtained from a Milli-Q water system was used in all experiments. All glassware were cleaned using freshly prepared aqua regia (HCl:HNO_3 in a 3:1 ratio by volume) followed by rinsing with copious amounts of water.

2.2 *Preparation of the seeds solution*

The seeds were prepared according to the method reported in our previous literature.[46,47] Briefly, 0.25 mL of 10 mM $HAuCl_4$ solution was added to 10 mL of 0.1 M CTAB solution in a 20 mL vial. After mixing the solution under stirring, 0.6 mL of an ice-cold, freshly prepared aqueous $NaBH_4$ solution (10 mM) was added all at once under vigorous stirring for 1 min. The resulting solution was kept in an

incubator at 30 °C and was used 30 min after its preparation. The concentration of the finally prepared seeds is 0.23 mM.

2.3 *Two-step seed-mediated synthesis of GNRs: Effects of varying growth times*

2.3.1 *Preparation of growth solutions A for two-step growth (bottles A)*: A 30 mL vial was used to mix 9.5 mL of 0.1 M CTAB, 4 mL of 50 mM NaOL, 1.25 mL of 10 mM $HAuCl_4$, 0.9 mL of 4 mM $AgNO_3$, and ultrapure water were mixed to make up the total volume to 25 mL. The solution was stirred at 700 rpm for 90 min at 30 °C using a constant-temperature magnetic stirrer, resulting in a colorless solution. 0.105 mL of HCl was added to adjust the pH of the solution, followed by slow stirring at 400 rpm for 15 min. Then, 62.5 μL of 64 mM AA solution was added, and the mixture was vigorously stirred for 30 s. Finally, 1.2 mL of seed solution was added to the vial, which was then left to stand at 30 °C in a constant-temperature magnetic stirrer for subsequent use. Spectrum changes in bottle A were recorded every 30 min (from 0 to 300 min). The final concentration of the seeds in bottle A is 11.04 μM.

2.3.2 *Preparation of growth solutions B for two-step growth (bottles B)*: A 30 mL vial was used to mix 9.5 mL of 0.1 M CTAB, 4 mL of 50 mM NaOL, 1.25 mL of 10 mM $HAuCl_4$, 0.9 mL of 4 mM $AgNO_3$, and ultrapure water were mixed to make up the total volume to 25 mL. The solution was stirred at 700 rpm for 90 min at 30 °C using a constant-temperature magnetic stirrer, resulting in a colorless solution. 0.105 mL of HCl was added to adjust the pH of the solution, followed by slow stirring at 400 rpm for 15 min. Then, 62.5 μL of 64 mM AA solution was added, and the mixture was vigorously stirred for 30 s. Finally, every 30 min, 0.5 mL of the solution A was added to each of the different vials, which were then left to stand at 30 °C in a constant-temperature magnetic stirrer. Spectrum changes in bottles B were recorded every 30 min (from 0 to 300 min).

2.4 *FDTD simulations*

To simulate the electric field intensity of GNRs, we employed the finite-difference time-domain FDTD method available in the commercial software FDTD Solution 8.19.1584 by Lumerical Solutions. We injected a pulsed light wave in the wavelength range of 400 to 1100 nm into a simulated box containing the GNRs to mimic the interaction between propagating plane waves and the nanorods. To accurately depict the system, we created an appropriately sized virtual boundary around the GNRs. The GNRs and the surrounding medium within the boundary were divided into a grid of 1 nm resolution to ensure simulation accuracy. The dimensions of the GNRs were obtained from the average values of TEM images. The refractive index of the surrounding medium was set to be 1.33 (water). This series of computations and simulation work provided a solid theoretical foundation and experimental data support for our research.

2.5 *Characterizations*

All extinction measurements were captured on a UV-1900i spectrophotometer (SHIMADZU, Japan) with a 10.0 mm optical path, whereby a glass cuvette filled with Milli-Q water was used as the reference. Transmission electron microscopy (TEM) images were captured on a HT-7700 microscope (HITACHI, Japan) operating at 100.0 kV.

3. Results and discussion

3.1 *Two-step growth method for synthesizing GNRs*

In the traditional two-step synthesis of GNRs, fresh reactants were added to the original growth solution after each step. In this experiment, a small portion of the growth solution was transferred to a new growth solution after each step to facilitate the subsequent growth, as illustrated in Figure 1(a). The seeds were prepared following the procedure outlined in a one-pot synthesis literature, where $HAuCl_4$ was reduced by freshly prepared strong reducing agent, sodium borohydride ($NaBH_4$). GNRs growth solution utilized a binary surfactant system composed of CTAB and sodium oleate (NaOL). NaOL, a sodium salt of long-chain unsaturated fatty acids, contains double bonds enabling slow reduction of $HAuCl_4$ in the absence of ascorbic acid (AA). In the seed-mediated growth method for GNRs, NaOL serves as a surfactant to regulate dimensional uniformity, monodispersity, and longitudinal surface plasmon resonance (LSPR) characteristics. Optimization of the NaOL-to-CTAB ratio allowed synthesis of GNRs with tunable aspect ratios. The first step of growth was accomplished by rapidly introducing 1.2 mL of 0.23 mM seed solution into growth solution (A). After incubation at 30 °C for

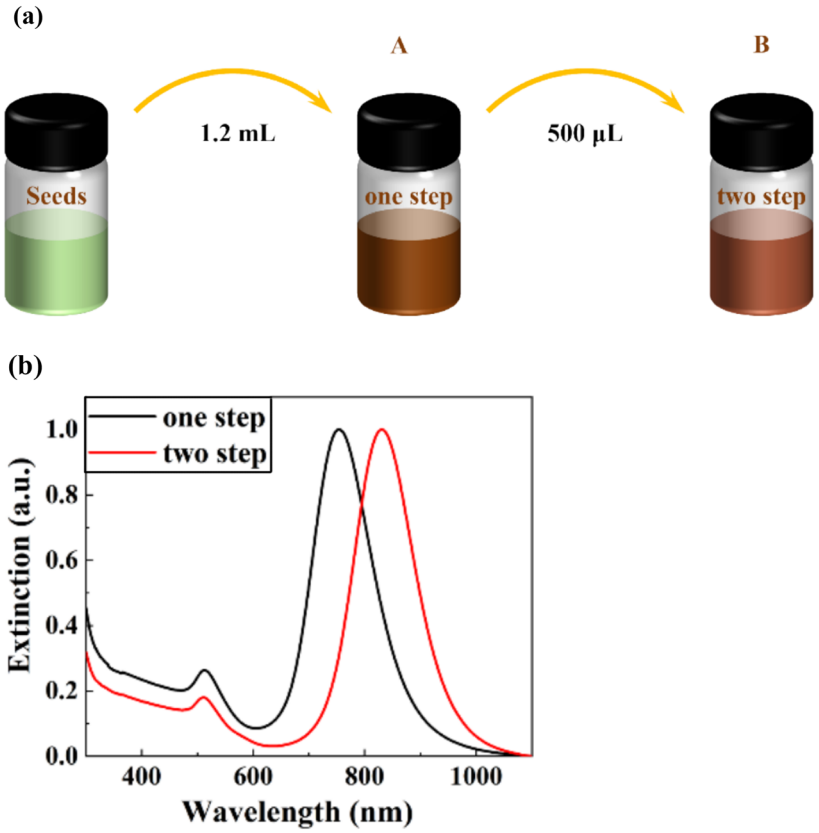

Figure 1. **(a)** Schematic diagram of the two-step seed-mediated method for growing GNRs. **(b)** Comparison of normalized extinction spectrum of GNRs grown via one-step and two-step methods.

30 min, 0.5 mL of the first-stage growth solution (A) was transferred to fresh growth solution (B) and thoroughly mixed. Compared with GNRs synthesized via the conventional one-step seed-mediated method, the two-step method-generated GNRs exhibited a red-shifted longitudinal localized surface plasmon resonance (LSPR) peak (from 754 to 830 nm), while the transverse localized surface plasmon resonance (TSPR) peak remained unchanged. Notably, Figure 1(b) demonstrates that the LSPR-to-TSPR (A_L/A_T) intensity ratio was significantly higher for GNRs prepared by the two-step method (5.56) compared to the one-step method (4.17). These results clearly indicate that the two-step method improves both the yield and uniformity of GNRs compared to those obtained through the single-step approach.

To investigate the effect of adding solution from bottle A into bottle B at different time points (every 30 min) on the growth process, GNRs were characterized using visible-NIR extinction spectroscopy, as shown in Supplementary Figure S1. It can be observed from the figure that, except for when the solution from bottle A was added at 0 min, there was almost no generation of GNRs in the solution in bottle B after 12 h. However, when the solution from bottle A was added at other time points (30–180 min), GNRs were generated in the solution in bottle B after 12 h. Additionally, the peak position and intensity of the extinction peaks were relatively close at these time points. Finally, through comprehensive analysis of the extinction peak characteristics, including peak intensity, FWHM, and the intensity ratio of A_L/A_T (peak value of the longitudinal peak/peak value of the transverse peak) as shown in Supplementary Table S1, the conclusion was drawn that adding the solution from bottle A into the solution in bottle B at 30 min resulted in the most ideal growth of GNRs. This research finding indicates that the selection of time points significantly influences the growth process of GNRs, with a 30-minute interval performing optimally under the experimental conditions. This short time interval effectively reduces time while ensuring quality.

During the growth process of solutions in bottle A and bottle B, we also recorded their growth at different time points (every 30 min), as shown in Figure 2. It can be observed that throughout the entire growth process, the extinction peaks of solutions in both bottles gradually intensified, while the entire spectrum exhibited a blue-shift trend. However, notably, the

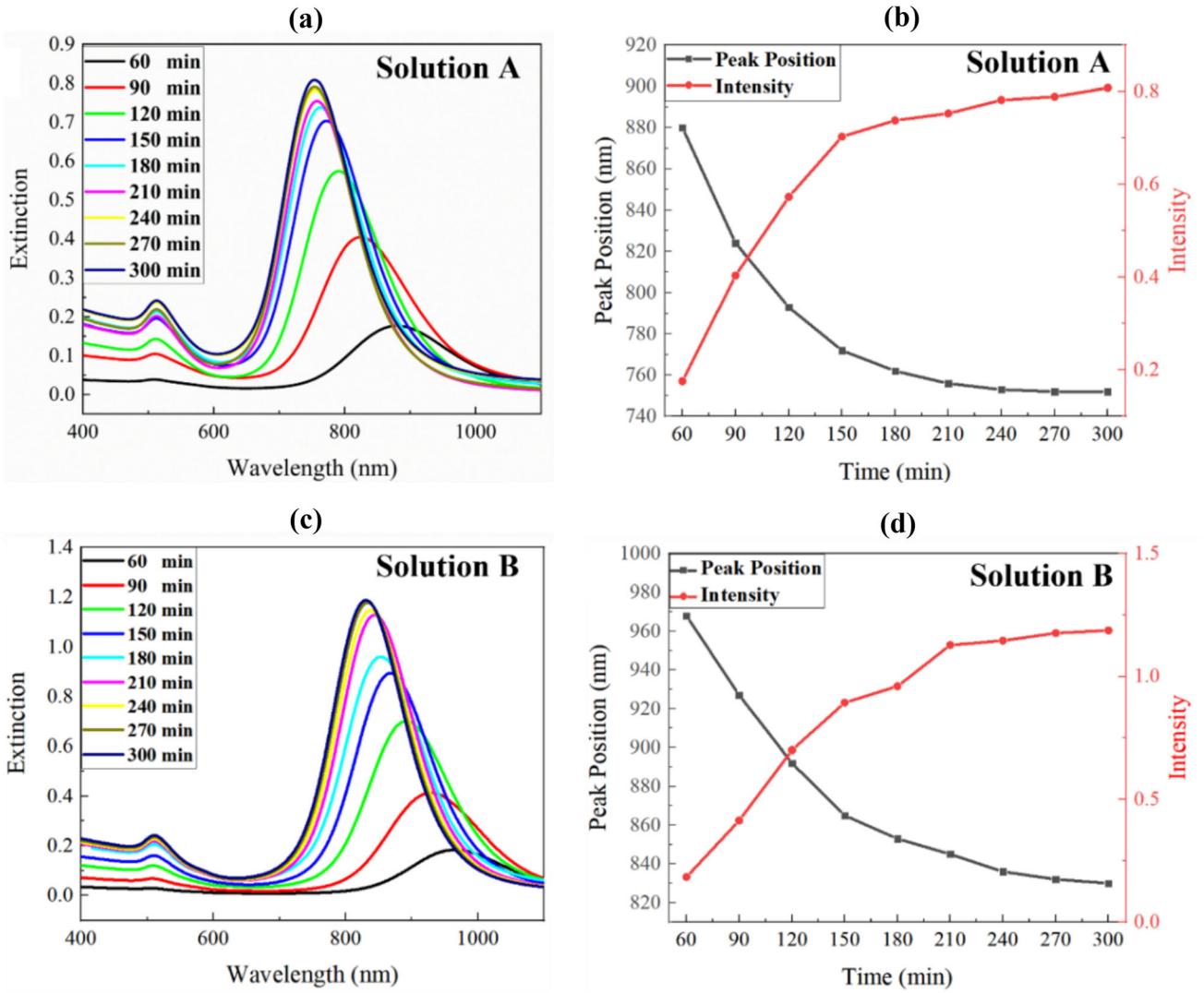

Figure 2. **(a)** Vis-NIR extinction spectrum of solution A during the growth process, **(b)** relationship between the peak position and intensity of the LSPR peak in solution A and growth time, **(c)** Vis-NIR extinction spectrum of solution B during the growth process, **(d)** relationship between the peak position and intensity of the LSPR peak in solution B and growth time, recorded at intervals of 30 min between 60–300 min.

stabilization time of the growth in solution A was approximately 150 min, which was about 1 h earlier than in solution B (approximately 210 min). Furthermore, when the growth of solution A nearly ceased, its extinction peak intensity was approximately 0.8, lower than that of solution B (approximately 1.2). This indicates that the two-step method required a longer growth duration than the one-step method, resulting in GNRs with larger sizes and higher aspect ratios. Additionally, when the growth time reached 300 min, solution A exhibited an extinction spectrum full width at half maximum (FWHM) of 123 nm, while solution B showed a smaller FWHM of 119 nm, solution A's A_L/A_T (4.17) was notably lower than that of solution B (5.56). In GNR spectra, smaller FWHM and larger A_L/A_T correlate with higher product yield and superior quality. These findings collectively demonstrate that the two-step method outperforms the one-step method in achieving both higher yield and better uniformity for GNR synthesis.

3.2 *Effects of seed quantity variation on GNRs synthesis in the first step of two-step growth*

In the two-step growth method, each individual step is analogous to the common one-step seed-mediated growth method. Hence, factors influencing GNRs growth in the one-step method might similarly affect the two-step method, such as seed volumes, silver content, pH of the growth solution, etc. Therefore, as a reference, after determining the optimal time interval

of 30 min for adding Solution A to Solution B, we initially investigated the influence of seed amount on the product in the one-step growth (Solution A), as shown in Supplementary Figure S2. As the seed amount increased from 40 to 5120 μL, the LSPR peak exhibited a red shift, followed by a blue shift as the seed volume further increased. Studies on the kinetics of GNRs growth suggest the existence of a longitudinal growth preference during the initial growth stage (Stage I), which gradually diminishes later (Stage II), resulting in an initial increase followed by a decrease in the aspect ratio of GNRs during growth. This observation can be explained as follows: At lower seed concentrations, the ratio of gold ions to seeds is relatively high, allowing each seed to elongate before widening, thereby forming GNRs with larger aspect ratios. As the seed concentration increases (from 40 to 320 μL), the ratio of gold ions to seeds decreases, causing both the length and width of the seeds to decrease. However, the width decreases more significantly because most gold ions are consumed during elongation (Stage I), resulting in a reduction in the final product size but an increase in the aspect ratio (corresponding to the red shift of the LSPR peak).

As the seed concentration continues to increase (from 320 to 2560 μL), the ratio of gold ions to seeds further decreases. Due to the low ratio of gold ions to seeds, seeds may not even complete the initial longitudinal growth in Stage I, leading to a decrease in size and aspect ratio (corresponding to the blue shift of the LSPR peak). However, when the seed volume is excessive (5120 μL), the ratio of gold ions to seeds

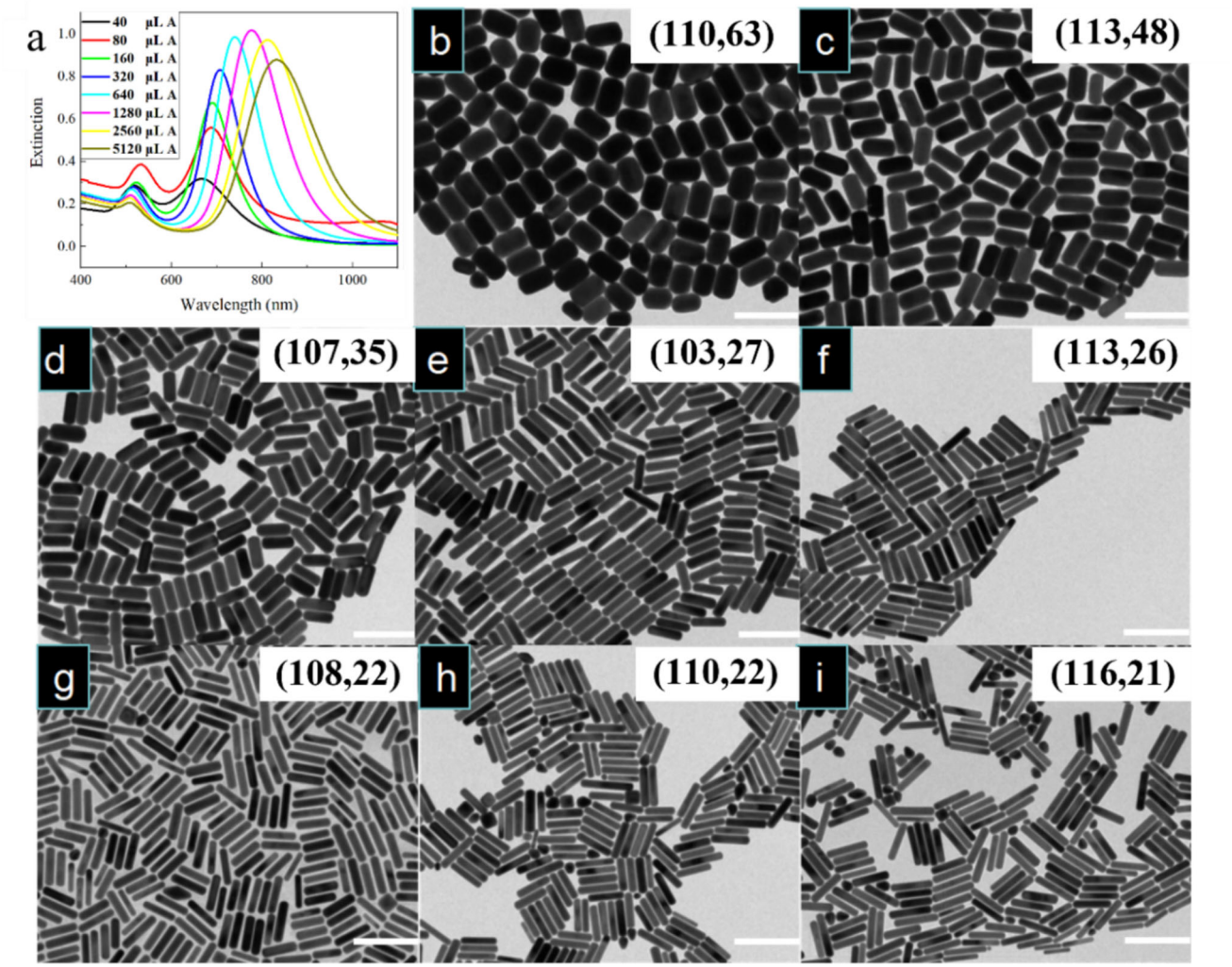

Figure 3. Influence of different volumes of seeds (11.04 μM) on the synthesis of GNRs in the second step of two-step growth. **(a)** Vis-NIR spectrum of the final products synthesized using different volumes of seeds: 40 μL (black), 80 μL (red), 160 μL (green), 320 μL (blue), 640 μL (cyan), 1280 μL (magenta), 2560 μL (yellow), and 5120 μL (dark yellow); **(b–i)** corresponding TEM images of the GNRs shown in (**a**) with increasing seed volumes from (**b–i**). All the scale bars are 200 nm. The average length and diameter of the GNRs are indicated on the top right corner of each image (units: nm).

decreases further. With limited gold ions compared to the abundant seeds, only few of seeds can grow into GNRs (resulting in a very low peak in the LSPR spectrum). This outcome highlights the significant impact of seed amounts on the GNRs growth process.

3.3 *Effects of seed quantity variation on GNRs synthesis in the second step of two-step growth*

Continuing, we have tested the effect of varying seed quantities during the second-step growth process on the final product. It is evident from the vis-NIR spectrum (Figure 3) that as the seed quantity increased from 40 to 5120 μL, the LSPR peak gradually red-shifted, shifting from 656 to 844 nm, covering a broad range from visible to near-infrared. In the two-step growth, an initial blue shift followed by a red shift of the LSPR peak with increasing seed quantity was observed, which seems inconsistent with the results of one-step growth. However, considering the dilution effect when transferring the first-step growth solution to the second-step growth solution, it still follows the same trend observed in one-step growth.

In the two-step growth, despite transferring first-step growth solutions (A) ranging from 40 to 5120 μL to the second-step growth Solution (B), they contained only 0.8 to 102.4 μL of original seeds because the seed solution was diluted by a factor of 50 when added to the first-step growth solution (0.5 mL of Solution A added to Solution B), falling within the range of seed quantity (< 320 μL) that resulted in the red shift of the LSPR peak in one-step growth. The obtained LSPR peak positions, intensities, FWHM, and corresponding A_L/A_T are listed in Table 1, where the overall FWHM of the LSPR peak is much smaller than that obtained in one-step growth (Supplementary Table S2), indicating improved optical uniformity of GNRs through the two-step growth. Representative TEM images of GNRs synthesized with different seed quantities in the second step are shown in Figure 3(b–i), where all products exhibit highly uniform GNRs shapes and sizes.

As the seed quantity increased from 40 to 5120 μL, there was almost no significant change in the length of the GNRs (remaining at approximately 110 nm), while the width decreased from 62.5 ± 4.8 nm to 21.3 ± 2.8 nm. The decrease in width was highly significant (295%) compared to almost no change in length, resulting in an increase in aspect ratio from 1.8 ± 0.1 to 5.6 ± 0.7, consistent with the red shift of the LSPR peak observed in the vis-NIR spectra (Figure 3). This result also aligns with the gradual widening of GNRs in Stage II after completing Stage I growth with increasing seed quantity, where insufficient gold ions are available to continue widening GNRs after Stage I growth (manifested as width reduction), thus gradually increasing the aspect ratio, leading to the red shift of the LSPR peak.

Detailed statistical data on the length, width, and aspect ratio of GNRs shown in Figure 3 are listed in Table 1. According to the data in the table, it can be observed that when the seed quantity is too low or too high, the synthesized GNRs exhibit poor monodispersity. This observation was also verified by the TEM images (Figure 3), where more impurities presented in these cases. Therefore, controlling the seed quantity is crucial for obtaining GNRs with good monodispersity and desired properties. An appropriate amount of seeds can effectively guide the growth of gold, ensuring the quality of the obtained GNRs.

3.4 *Effects of pH variation on GNRs synthesis in the first step of two-step growth*

According to previous studies,[46,47] the pH value of the growth solution was crucial for the uniformity of GNRs in one-step synthesis. At low pH values (e.g., 1–2), the

Table 1. LSPR, FWHM, size, aspect ratio (AR) and aspect ratio along long axis (A_L/A_T) of GNRs synthesized using different volumes of seeds.

Seeds (μL)	LSPR (nm)	FWHM (nm)	Length (nm)	Width (nm)	AR	A_L/A_T
40	668	166	110 ± 4.4	62.5 ± 4.8	1.8 ± 0.1	1.11
80	688	115	113 ± 3.7	48 ± 4.3	2.4 ± 0.3	1.45
160	691	100	106.9 ± 3	35.3 ± 3.5	3.1 ± 0.3	2.25
320	707	100	103.6 ± 3.1	27.4 ± 2.9	3.8 ± 0.4	2.96
640	740	114	113 ± 4.9	25.7 ± 2.8	4.3 ± 0.5	3.68
1280	775	128	107.9 ± 3.8	22.7 ± 2.7	4.8 ± 0.5	4.39
2560	812	159	110.5 ± 3.5	22 ± 2.8	5.1 ± 0.6	4.27
5120	832	170	116.1 ± 10.1	21.3 ± 2.8	5.6 ± 0.7	4.25

reduction reaction was slow, with gold atoms preferentially depositing at the tips of seed particles, promoting longitudinal growth and forming rod-like structures with high aspect ratios; high pH values may induce lateral facet growth, leading to increased nanorod diameters or irregular morphologies. Therefore, it is necessary to investigate its influence on the two-step growth process. We first examined how the pH in the first step affects the uniformity of GNRs, while keeping the pH value unchanged in the second step. The results are shown in Supplementary Figure S3. Except for instances at 25 and 50 μL where the higher pH values in the first step led to overly rapid growth and consequently poorer quality of synthesized GNRs, products synthesized at different pH values exhibited similar extinction peaks. This indicates that we obtained GNRs with similar aspect ratios, implying that the variation in pH values in the first step has limited influence on the final product. Throughout the growth process, the spectra continuously red-shifted with decreasing pH values, consistent with our observations in one-step growth, where the LSPR peak initially red-shifted as pH decreased. However, the overall spectra fluctuation range was small, only oscillating between 800 and 850 nm, indicating that the second-step growth eliminated the variations caused by pH in the first step, even though the addition of HCl led to a red shift in the longitudinal LSPR peak of GNRs. However, due to dilution effects upon addition to the second step, the red shift was only a few tens of nanometers. This result suggests that the two-step method, while dynamically controlling pH, eliminates fluctuations from the first step through the second-step growth process, providing more controllable conditions for obtaining stable and uniform GNRs.

As HCl gradually increased, except for the influence of 25 μL on the overall effect, changes in the LSPR peak exhibited a certain trend. As shown in Supplementary Figure S3, with increasing HCl addition (except for the influence at 25 μL), the LSPR peak exhibited a distinct trend: continuous red-shift (from 50 to 200 μL). The FWHM of GNRs showed a different pattern: initially decreasing with HCl addition (from 50 to 75 μL), then increasing (from 70 to 150 μL), and finally decreasing continuously (from 150 to 200 μL). Additionally, the A_L/A_T ratio demonstrated a sequential variation: rising with HCl addition (from 25 to 100 μL), declining (from 100 to 150 μL), and then increasing again (from 150 to 200 μL). These three parameters (peak, FWHM, A_L/A_T) reflect the yield, size uniformity, and purity of the GNRs (Supplementary Table S3). Overall, considering these trends, the addition of HCl in the first step appears to reach an optimal state at 200 μL, providing favorable conditions for obtaining GNRs with high yield, size uniformity, and purity.

3.5 *Effects of pH variation on GNRs synthesis in the second step of two-step growth*

Furthermore, we investigated how the pH in the second step affects the synthesis of GNRs while keeping the pH in the first step constant (100 μL). The vis-NIR spectra of the synthesized GNRs are shown in Figure 4, with decreasing pH (increasing HCl dosage), the LSPR peak of the final product gradually red-shifted from 644 to 1020 nm, consistent with observations in conventional one-step growth. This phenomenon arises because the gradual pH decrease elevates H concentration in the solution, inhibiting ascorbic acid (AA) hydrolysis and slowing the reaction rate. The reduced reaction rate favors anisotropic growth over homogeneous nucleation, leading GNRs to predominantly elongate axially and increasing their aspect ratio.

During this process, the FWHM exhibited a gradual increase from 50 to 200 μL. Simultaneously, the A_L/A_T ratio initially rose (25–125 μL) and then declined (125–200 μL) with HCl addition. By synthesizing peak position, FWHM, and A_L/A_T ratio trends, the optimal pH for the two-step method aligns with the previously reported optimal pH (100 μL) for one-step synthesis (Table 2). These findings demonstrate that pH regulation effectively modulates GNR size and optical properties, offering a versatile strategy for tailoring GNRs to specific applications.

3.6 *Effects of silver ion concentration variation on GNRs synthesis in the first step of two-step growth*

To explore the role of silver ions in the two-step growth of GNRs, we separately investigated the effects of silver ion concentration in the first and second steps on the final product. A 30 mL vial was used to mix 9.5 mL 0.1 M CTAB, 4 mL 50 mM NaOL, 1.25 mL 10 mM $HAuCl_4$, 0.9 mL of 4 mM $AgNO_3$, and ultrapure water were mixed to make up the total volume to 25 mL. Initially, the silver ion concentration in the second step was fixed (0.9 mL), while the silver ion quantity in the first step was varied (0–1.8 mL). Supplementary Figure S4 illustrates the vis-NIR spectrum of the final products after two-step growth. When there were no silver ions in the first step, even in the presence of silver ions in the second step, the final products remained close to spherical (with only one peak at 560 nm). However, when silver ions were

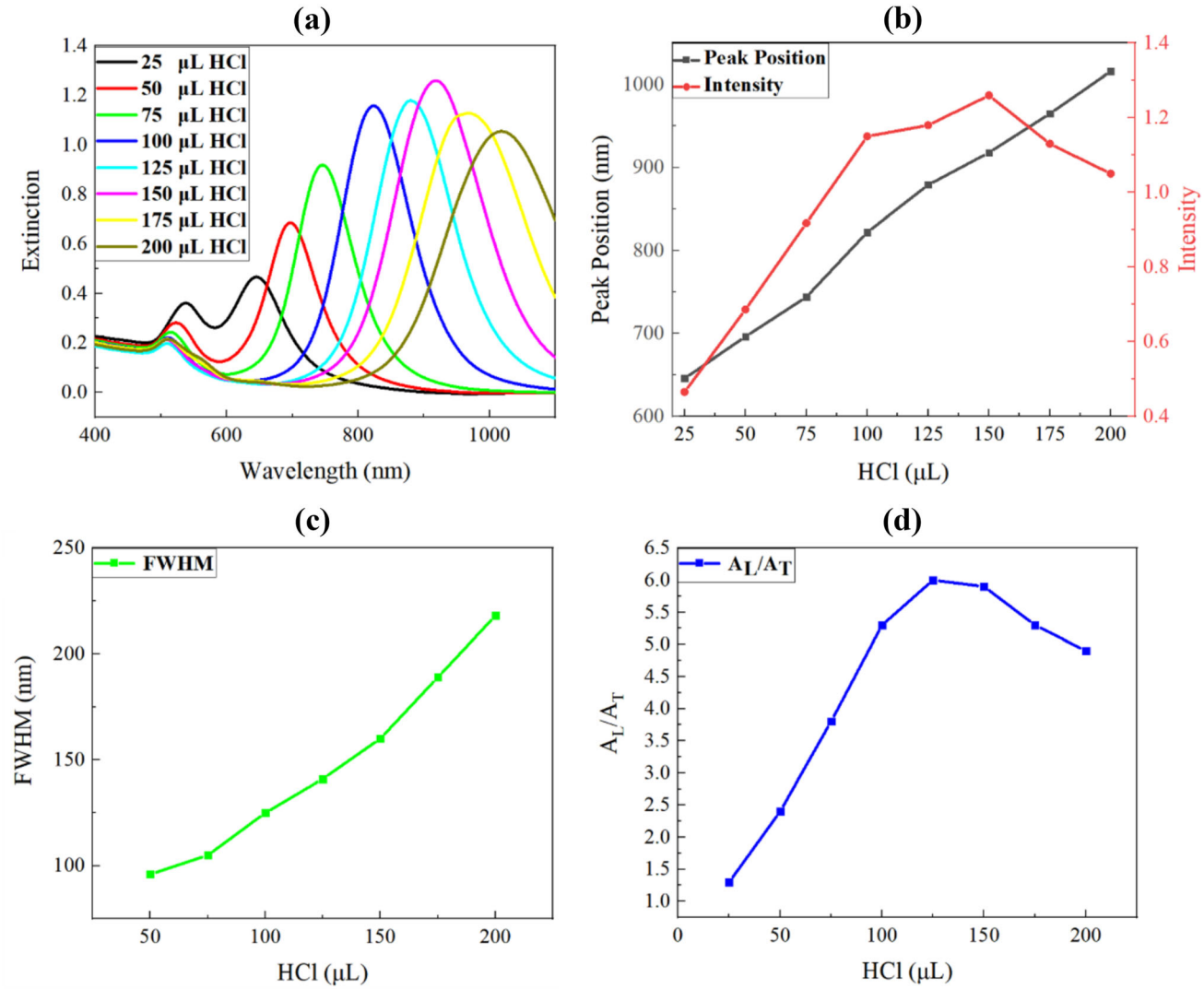

Figure 4. UV-Vis extinction spectrum **(a)** and the corresponding changes in LSPR peak wavelength and intensity **(b)**, full width at half maximum (FWHM) **(c)**, and A_L/A_T **(d)** with variations in the HCl (37 wt.% in water) of solution in bottle B.

Table 2. Vis-NIR extinction spectrum data of the solution in bottle B under different pH values.

HCl (µL)	Peak (nm)	Intensity	FWHM (nm)	A_L/A_T
25	646	0.466	—	1.3
50	696	0.686	96	2.4
75	744	0.918	105	3.8
100	822	1.15	125	5.3
125	879	1.18	141	6
150	918	1.26	160	5.9
175	965	1.13	189	5.3
200	1016	1.05	218	4.9

presented in the first step, the final products were all nanorods. It is known from the literature based on extensive TEM investigation that symmetry breaking of isotropic seeds take place early in the synthesis of AuNRs.[48,49] As shown in Supplementary Table S4, as the silver ion concentration in the first step increased (0–1.8 mL), the aspect ratio of GNRs initially increased and then decreased, reflected in the vis-NIR spectra by a red shift in the LSPR (0–1.2 mL) followed by a blue shift (1.2–1.8 mL). Since silver ions play a crucial role in breaking the symmetry of the seeds during the growth of GNRs, and the critical size of symmetrically broken seeds is closely related to the concentration of silver ions in the growth solution, when the silver ion concentration is too high, they accelerate the symmetry breaking of seed particles, resulting in the formation of shorter and wider GNRs, thus reducing the aspect ratio.[50]

3.7 *Effects of silver ion concentration variation on GNRs synthesis in the second step of two-step growth*

Next, we tested the effect of silver ion concentration in the second step (0–3 mL) while keeping the silver ion

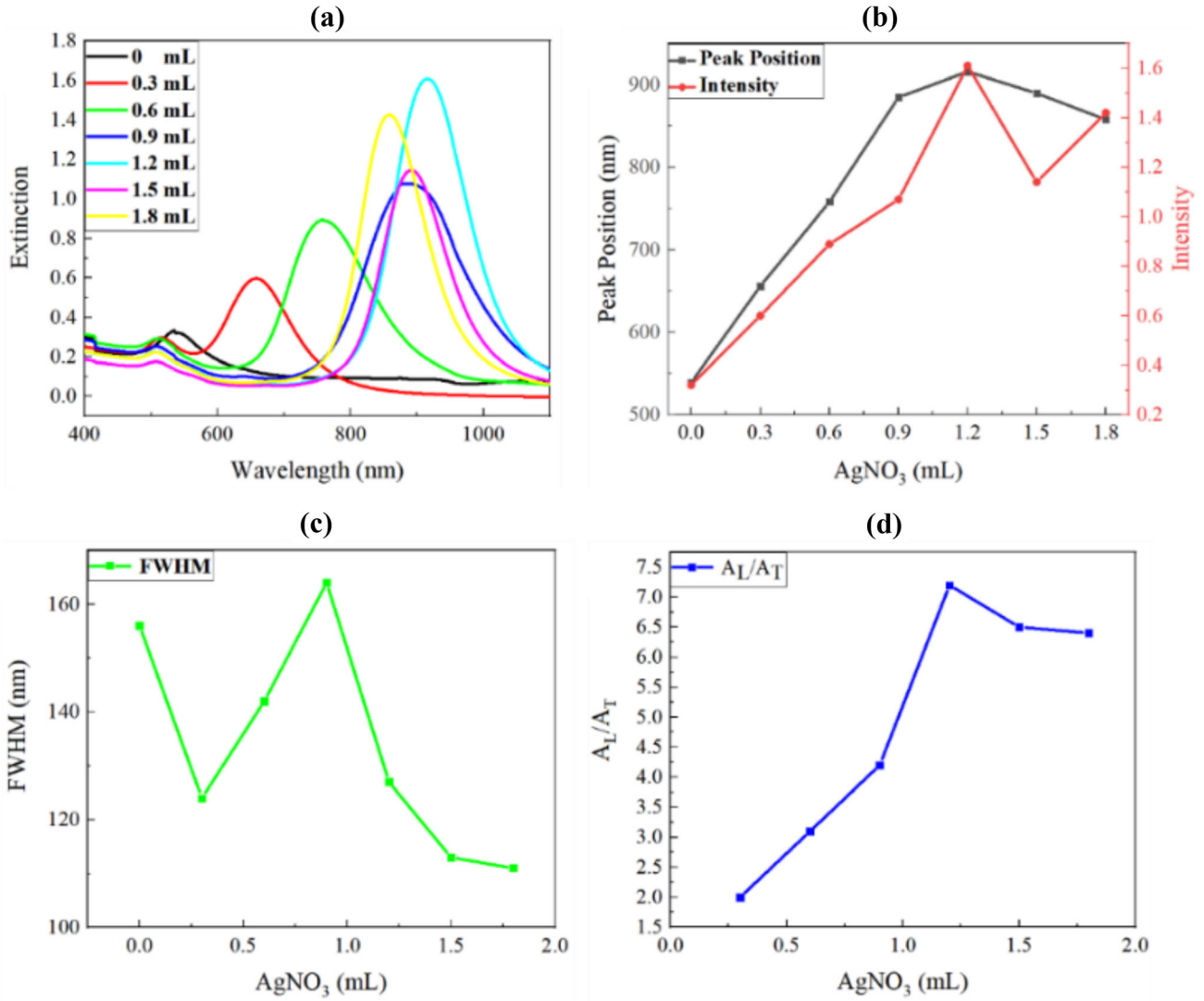

Figure 5. **(a)** Vis-NIR extinction spectra of the solution in bottle B with varying silver content. **(b)** Changes in LSPR peak position and intensity with adjustments in silver content in the solution in bottle B. **(c)** Variation in FWHM with adjustments in silver content in the solution in bottle B. **(d)** Changes in A_L/A_T with adjustments in silver content in the solution in bottle B.

concentration in the first step unchanged (0.9 mL), and the results were shown in Figure 5. When no silver ions were presented in the second step, the product was similar to the final product obtained from the first step alone (with only one peak at 536 nm). As the silver ion concentration increased gradually from 0.3 to 1.2 mL, and then from 1.2 to 2.1 mL, the vis-NIR spectra results were similar as those obtained by adjusting the silver ion concentration in the first step. By comparing the results of changing the silver ion concentration in the first and second steps, we can draw the following conclusions. Firstly, silver ions are not only crucial for the early-stage symmetry breaking of seed growth but also affect the subsequent growth leading to the formation of large GNRs. In the absence of silver ions in the second growth step, the product reverts to a spherical shape after the symmetry-breaking event. Secondly, the regulation of the aspect ratio of GNRs by silver ions is not a linear change; too much or too little silver ions can lead to a decrease in the monodispersity of the grown GNRs (increased FWHM). Considering the peak, FWHM, and A_L/A_T ratio together, the optimal silver nitrate concentration in the second step of the two-step method should be 1.2 mL, consistent with the requirement in the first step. Considering the peak, FWHM, and A_L/A_T ratio together (Table 3), the optimal silver nitrate concentration in the first step of the two-step method should be 1.2 mL. The quantities of seeds, pH, and silver ions were adjusted in the first and second steps

Table 3. Vis-NIR extinction spectra data of the solution in bottle B under different silver ion concentrations.

$AgNO_3$ (mL)	Peak (nm)	Intensity	FWHM (nm)	A_L/A_T
0	539	0.32	156	—
0.3	656	0.61	124	2
0.6	758	0.89	142	3.1
0.9	885	1.07	164	4.2
1.2	916	1.61	127	7.2
1.5	890	1.61	113	6.5
1.8	858	1.42	111	6.4

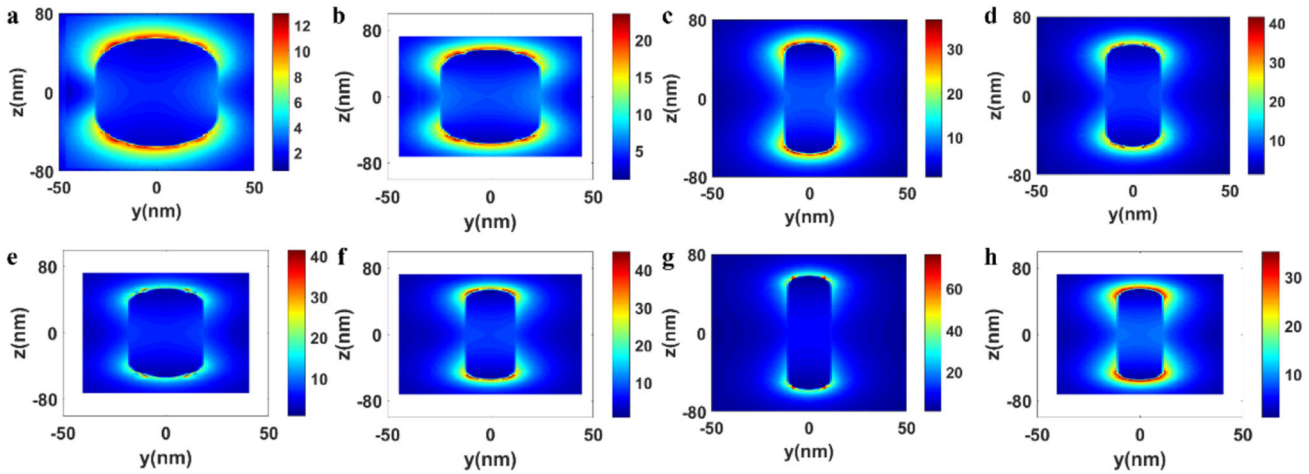

Figure 6. Electric field intensity maps obtained from simulations of GNRs with different sizes.

respectively, with the experimental data detailed in Supplementary Tables S6 and S7.

3.8 *Finite-difference time-domain (FDTD) simulations*

The FDTD simulations were employed to compute the electric field intensity of GNRs with different dimensions. The simulations were conducted using the commercial software Lumerical Solutions. Symmetric (in the X-axis direction) and anti-symmetric (in the Z-axis direction) boundary conditions were applied, with perfect boundary conditions in the Z-direction. A plane wave source was chosen as the light source, and the wavelength range of the simulation was set from 400 to 1100 nm. Supplementary Figure S5 illustrates the extinction spectrum of individual GNRs calculated based on the experimental measured dimensions in Supplementary Table S1. As the aspect ratio of the GNRs increases, the LSPR peak gradually red-shifts, consistent with the experimental results. Figure 6 depicts the electric field intensity maps of GNRs with different sizes, indicating the formation of electromagnetic hotspots near the tips of the nanorods. The study reveals that the electric field intensity of GNRs exhibits a trend of initially increasing and then decreasing as the aspect ratio of the nanorods gradually increases, as shown in Supplementary Table S5.

4. Conclusions

In conclusion, we developed a two-step seed-mediated synthesis method to successfully prepare well-dispersed and uniformly shaped GNRs with tunable LSPRs ranging from 668 to 1020 nm. In terms of optimization of growth conditions, we determined that the best conditions were to perform the first step of the synthesis for 30 min before the second step of the synthesis. We also recorded the growth progression of the A-vial solution and the B-vial solution at

30-minute intervals over a 300-minute period, clarifying the point at which growth essentially stops for both steps. We investigated the effects of seed volume, pH, and silver content on GNR growth. The optimal conditions were determined to be adding 1280 μL of seed solution to bottle A and adding 0.5 mL of solution from bottle A to bottle B. The two-step synthesis was performed in the same manner. In the two-step synthesis, changing the pH in the second step was more effective in changing the morphology of GNRS because only a small amount of the solution from the first step was used in the second step of the two-step synthesis. Changes in the silver ion content in the two steps also affected the LSPR peak of the GNRs, with the peak shifting red initially and then blue. This may be attributed to the acceleration of the symmetry breaking of seed particles due to silver ions exceeding the critical concentration, resulting in the formation of shorter and wider GNRs, reducing the aspect ratio. Through FDTD simulations, the relationship between the aspect ratio variation of the GNRs and the extinction spectra as well as the electric field intensity were investigated. The simulated results demonstrated that as the aspect ratio of the GNRs increased, their LSPRs gradually redshifted, while the electric field intensity exhibited a trend of initially increasing and then decreasing. Therefore, preparing GNRs with an appropriate aspect ratio is an effective means to enhance the electric field intensity of the GNRs. Due to the similarity in synthesis methods, this two-step approach is expected to be applicable to the synthesis of other shapes of gold nanoparticles, such as triangles, cubes, tetrahedrons, and bipyramids.

Acknowledgements

We thank Sudan Shen for her assistance in TEM at State Key Laboratory of Chemical Engineering (Zhejiang University). We also acknowledge financial support from Zhejiang Provincial Natural Science Foundation (Grant: LY24F050008), and National Natural Science Foundation of China (NSFC, Grant: 61905056).

References

1. Mitiche S, Gueffrache S, Marguet S, Audibert J F, Pansu R B and Palpant B 2022 Coating gold nanorods with silica prevents the generation of reactive oxygen species under laser light irradiation for safe biomedical applications *J. Mater. Chem. B* **10** 589
2. Roach L, Booth M E, Ingram N, Paterson D A, Batchelor D V B, Moorcroft S C T, Bushby R J, Critchley K, Coletta P L and Evans S D 2021 Evaluating phospholipid-functionalized gold nanorods for *in vivo* applications *Small 17* 2006797 https://doi.org/10.1002/smll.202006797
3. Zhang J F, Yin X F, Li C C, Yin X L, Xue Q H, Ding L, Ju J L, Ma J F, Zhu Y, Du D S, Reis R L and Wang Y L 2022 A multifunctional photoacoustic/fluorescence dual-mode-imaging gold-based theranostic nanoformulation without external laser limitations *Adv. Mater.* **34** 2110690
4. Deinavizadeh M, Kiasat A R, Hooshmand N, Labouta H I, Shafiei M, Sabaeian M, Mirzajani R, Zahraei S M, Makvandi P and El-Sayed M A 2023 Near-infrared/pH dual-responsive nanosponges encapsulating gold nanorods for synergistic chemo-phototherapy of lung cancer *ACS Appl. Nano Mater.* **6** 16332
5. Liu X D, Chen B, Wang G G, Ma S, Cheng L, Liu W, Zhou L and Wang Q Q 2021 Controlled growth of hierarchical Bi_2Se_3/CdSe-Au nanorods with optimized photothermal conversion and demonstrations in photothermal therapy *Adv. Funct. Mater.* **31** 2104424
6. Zhao Y H, Sarhan R M, Eljarrat A, Kochovski Z, Koch C, Schmidt B, Koopman W and Lu Y 2022 Surface-functionalized Au-Pd nanorods with enhanced photothermal conversion and catalytic performance *ACS Appl. Mater. Interfaces* **14** 17259
7. Li F, Wang K, Deng N X, Xu J P, Yi M D, Xiong B J and Zhu J T 2021 Self-assembly of polymer end-tethered gold nanorods into two-dimensional arrays with tunable tilt structures *ACS Appl. Mater. Interfaces* **13** 6566
8. Li J Y, Wuenschell J, Li Z, Bera S, Liu K, Tang R H, Du H, Ohodnicki P R and Shen S 2021 Fiber coupled near-field thermoplasmonic emission from gold nanorods at 1100 K *Small 17* 2007274
9. Zhang N N, Shen Z L, Gao S Y, Peng F, Cao Z J, Wang Y, Wang Z Z, Zhang W, Yang Y, Liu K and Sun T M 2023 Synthesis and plasmonic chiroptical properties of double-helical gold nanorod enantiomers *Adv. Opt. Mater.* **11** 2203119
10. Guo J Q, Wu F, Song G, Huang Y M, Jiao R Z and Yu L 2021 Diverse axial chiral assemblies of J-aggregates in plexcitonic nanoparticles *Nanoscale* **13** 15812
11. Huang M, Ali W, Yang L L, Huang J H, Yao C D, Xie Y F, Sun R H, Zhu C G, Tan Y K, Liu X, Li S M, Li Z W and Pan A L 2023 Multifunctional optoelectronic synapses based on arrayed MoS_2 monolayers emulating human association memory *Adv. Sci. 10* 2300120
12. Liu X D, Chen Z Y, Liu Q K, Sheetah G H, Sun N F, Zhao P, Xie Y and Smalyukh I I 2021 Morphological and orientational controls of self-assembly of gold nanorods directed by evaporative microflows *ACS Appl. Mater. Interfaces* **13** 53143
13. Baaske M D, Asgari N, Punj D and Orrit M 2022 Nanosecond time scale transient optoplasmonic detection of single proteins *Sci. Adv. 8* eabl5576
14. Meireles I, Cipreste M F, Gastelois P L, Macedo W A D, Gomes D A and de Sousa E M B 2021 Synthesis and characterization of gold nanorods coated by mesoporous silica MCM-41 as a platform bioapplication in photohyperthermia *Nanotechnology 32* 505720
15. Rizvi M H, Wang R S, Schubert J, Crumpler W D, Rossner C, Oldenburg A L, Fery A and Tracy J B 2022

Magnetic alignment for plasmonic control of gold nanorods coated with iron oxide nanoparticles *Adv. Mater.* **34** 2203366
16. He S Y, Jiang B B, Wang C Y, Chen C J, Duan H C, Jin S, Ye H Q, Lu L and Du K 2021 High reversible strain in nanotwinned metals *ACS Appl. Mater. Interfaces* **13** 46088
17. Lu J, Xue Y, Bernardino K, Zhang N N, Gomes W R, Ramesar N S, Liu S H, Hu Z, Sun T M, de Moura A F, Kotov N A and Liu K 2021 Enhanced optical asymmetry in supramolecular chiroplasmonic assemblies with long-range order *Science* **371** 1368
18. Velimirovic M, Pancaro A, Mildner R, Georgiou P G, Tirez K, Nelissen I, Johann C, Gibson M I and Vanhaecke F 2021 Characterization of gold nanorods conjugated with synthetic glycopolymers using an analytical approach based on spICP-SFMS and EAF4-MALS *Nanomaterials 11* 2720
19. Ding W H, Chen Z C A, Gu Y Y, Chen Z R, Zheng Y Q and Sun F 2021 Magnetic testis targeting and magnetic hyperthermia for noninvasive, controllable male contraception via intravenous administration *Nano Lett.* **21** 6289
20. Rincón-Iglesias M, Rodrigo I, Berganza L B, Abu Serea E S, Plazaola F, Lanceros-Méndez S, Lizundia E and Reguera J 2022 Core-shell Fe_3O_4@Au nanorod-loaded gels for tunable and anisotropic magneto- and photothermia *ACS Appl. Mater. Interfaces* **14** 7130
21. Fordey T, Bouchal P, Schovánek P, Baránek M, Bouchal Z, Dvorák P, Hrton M, Rovenská K, Ligmajer F, Chmelík R and Sikola T 2021 Single-shot three-dimensional orientation imaging of nanorods using spin to orbital angular momentum conversion *Nano Lett.* **21** 7244
22. Kim M, Vanderlaan D, Lee J, Choe A, Kubelick K P, Kim J and Emelianov S Y 2023 Hyper-branched gold nanoconstructs for photoacoustic imaging in the near-infrared optical window *Nano Lett.* **23** 9257
23. Salah D, Moghanm F S, Arshad M, Alanazi A A, Latif S, El-Gammal M I, Shimaa E M and Elsayed S 2021 Polymer-peptide modified gold nanorods to improve cell conjugation and cell labelling for stem cells photoacoustic imaging *Diagnostics* **11** 1196
24. Chu S Y, Wu M J, Yeh T H, Lee C T and Lee H Y 2023 Sensing mechanism and characterization of NO_2 gas sensors using gold-black NP-decorated Ga_2O_3 nanorod sensing membranes *ACS Sens. 9* 118
25. Liang Z H, Zhao J Y, Wang P L, Nie Y X, Xu S P and Ma Q 2022 Gold nanorod vertical array-based electrochemiluminescence polarization assay for triple-negative breast cancer detection *Anal. Chem.* **94** 1221
26. Meyer S M and Murphy C J 2022 Anisotropic silica coating on gold nanorods boosts their potential as SERS sensors *Nanoscale* **14** 5214
27. Chen Y X, Chen X H, Wu D, Xin H H, Chen D S, Li D, Pan H M, Zhou C X and Ping Y 2021 Delivery of CRISPR/Cas_9 plasmids by cationic gold nanorods: impact of the aspect ratio on genome editing and treatment of hepatic fibrosis *Chem. Mater.* **33** 81
28. Qamar M, Abbas G, Afzaal M, Naz M Y, Ghuffar A, Irfan M, Legutko S, Jozwik J, Zawada-Michalowska M, Ghanim A A J, Rahman S, Niazi U M, Jalalah M, Alkahtani F S, Khan M K A and Kosicka E 2022 Gold nanorods for doxorubicin delivery: numerical analysis of electric field enhancement, optical properties and drug loading/releasing efficiency *Materials* **15** 1764
29. Refaat A, del Rosal B, Palasubramaniam J, Pietersz G, Wang X W, Moulton S E and Peter K 2021 Near-infrared light-responsive liposomes for protein delivery: Towards bleeding-free photothermally-assisted thrombolysis *J. Control. Release* **337** 212
30. González-Rubio G, Kumar V, Llombart P, Díaz-Núñez P, Bladt E, Altantzis T, Bals S, Peña-Rodríguez O, Noya E G, MacDowell L G, Guerrero-Martínez A and Liz-Marzán L M 2019 Disconnecting symmetry breaking from seeded growth for the reproducible synthesis of high quality gold nanorods *ACS Nano* **13** 4424
31. Sánchez-Iglesias A, Winckelmans N, Altantzis T, Bals S, Grzelczak M and Liz-Marzán L M 2017 High-yield seeded growth of monodisperse pentatwinned gold nanoparticles through thermally induced seed twinning *J. Am. Chem. Soc.* **139** 107
32. Sau T K and Murphy C J 2004 Seeded high yield synthesis of short Au nanorods in aqueous solution *Langmuir* **20** 6414
33. Ye X C, Jin L H, Caglayan H, Chen J, Xing G Z, Zheng C, Doan-Nguyen V, Kang Y J, Engheta N, Kagan C R and Murray C B 2012 Improved size-tunable synthesis of monodisperse gold nanorods through the use of aromatic additives *ACS Nano* **6** 2804
34. Scarabelli L, Sánchez-Iglesias A, Pérez-Juste J and Liz-Marzán L M 2015 A "tips and tricks" practical guide to the synthesis of gold nanorods *J. Phys. Chem. Lett.* **6** 4270
35. Asgari N, Baaske M D and Orrit M 2023 Burst-by-burst measurement of rotational diffusion at nanosecond resolution reveals hot-brownian motion and single-chain binding *ACS Nano* **17** 12684
36. Deska R, Obstarczyk P, Matczyszyn K and Olesiak-Banska J 2021 Circular dichroism of gold bipyramid dimers *J. Phys. Chem. Lett.* **12** 5208
37. Vikas, Kumar R and Soni S 2022 Investigation of the plasmonic interaction of gold nanoparticles toward plasmonic photothermal therapeutics *Plasmonics 17* 107
38. Huang C L, Zhao H H, Peng Z X, Zheng B A, Zhang C and Wang J 2021 One-step fabrication of highly dense gold nanoparticles on polyamide for surface-enhanced Raman scattering *Appl. Surf. Sci.* **561** 149856
39. Pu H B, Huang Z B, Xu F and Sun D W 2021 Two-dimensional self-assembled Au -Ag core-shell nanorods nanoarray for sensitive detection of thiram in apple using surface-enhanced Raman spectroscopy *Food Chem.* **343** 128548

40. Harper-Harris J, Kant K and Singh G 2021 Oleic acid-assisted synthesis of tunable high-aspect-ratio multiply-twinned gold nanorods for bioimaging *ACS Appl. Nano Mater.* **4** 3325
41. Hwang H, Oh H and Song H Y J 2023 Shaping copper oxide layers on gold nanoparticle ensembles by controlled electrodeposition with single particle scatterometry *Small* **19** 2301241
42. Li M, Zhang Q, Huang H T, Zhang S T, Zhou L and Wang Q Q 2021 Three-step seedless synthesis of ultralong gold nanorods *Opt. Mater.* **116** 111095
43. Wang Y N, Wei W T, Yang C W and Huang M H 2013 Seed-mediated growth of ultralong gold nanorods and nanowires with a wide range of length tunability *Langmuir* **29** 10491
44. Vreeland E C, Watt J, Schober G B, Hance B G, Austin M J and Price A D, Fellows B D, Monson T C, Hudak N S, Maldonado-Camargo L, Bohorquez A C, Rinaldi C and Huber D L 2015 Enhanced nanoparticle size control by extending LaMer's mechanism *Chem. Mater.* **27** 6059
45. Busbee B D, Obare S O and Murphy C J 2003 An improved synthesis of high-aspect-ratio gold nanorods *Adv. Mater.* **15** 414
46. Wei M Z, Deng T S, Zhang Q, Cheng Z and Li S 2021 Seed-mediated synthesis of gold nanorods at low concentrations of CTAB *ACS Omega* **6** 9188
47. Wei M Z, Deng T S, Zhang Q, Chen X, Cheng Z, Li S and Gu Y-J 2022 New rule and growth model for the synthesis method of gold nanorods with binary surfactant CTAB and NaOL *AIP Adv.* **12** 085019
48. Walsh M J, Barrow S J, Tong W, Funston A M and Etheridge J 2015 Symmetry breaking and silver in gold nanorod growth *ACS Nano* **9** 715
49. Walsh M J, Tong W, Katz-Boon H, Mulvaney P, Etheridge J and Funston A M 2017 A mechanism for symmetry breaking and shape control in single-crystal gold nanorods *Acc. Chem. Res.* **50** 2925
50. Tong W M, Walsh M J, Mulvaney P, Etheridge J and Funston A M 2017 Control of symmetry breaking size and aspect ratio in gold nanorods: Underlying role of silver nitrate *J. Phys. Chem. C* **121** 3549